# Transforming Auxetic Metamaterials into Superhydrophobic Surfaces

MCHALE, Glen, ALDERSON, Andrew <http://orcid.org/0000-0002-6281-2624>, ARMSTRONG, Steven, MANDHANI, Shruti, MEYARI, Mahya, WELLS, Gary G., CARTER, Emma, LEDESMA-AGUILAR, Rodrigo, SEMPREBON, Ciro and EVANS, Kenneth E.

Available from Sheffield Hallam University Research Archive (SHURA) at:

https://shura.shu.ac.uk/33029/

# Transforming Auxetic Metamaterials into Superhydrophobic Surfaces

*Glen McHale, Andrew Alderson, Steven Armstrong, Shruti Mandhani, Mahya Meyari, Gary G. Wells, Emma Carter, Rodrigo Ledesma-Aguilar,\* Ciro Semprebon, and Kenneth E. Evans*

Superhydrophobic materials are often inspired by nature, whereas metamaterials are engineered to have properties not usually occurring naturally. In both, the key to their unique properties is structure. Here, it is shown that a negative Poisson's ratio (auxetic) mechanical metamaterial can transform into a unique superhydrophobic material. When stretched, its surface has the counterintuitive property that it also expands in the orthogonal lateral direction. The change in the solid surface fraction as strain is applied is modeled, and it is shown that it decreases as the space between solid elements of the auxetic lattice expands. This results in a unique dependence of the superhydrophobicity on strain. Experimental models are constructed to illustrate the relationship between different states of strain and superhydrophobicity as the lattice transitions from an auxetic to a conventional structure. The findings offer a new approach to designing superhydrophobic materials for self-cleaning surfaces, droplet transportation, droplet encapsulation, and oil–water separation.

G. McHale, S. Armstrong, M. Meyari, G. G. Wells, R. Ledesma-Aguilar
Wetting, Interfacial Science & Engineering Laboratory, Institute for Multiscale Thermofluids
The University of Edinburgh
Edinburgh EH9 3FD, Scotland, UK
E-mail: Rodrigo.Ledesma@ed.ac.uk

A. Alderson, S. Mandhani, E. Carter
Materials & Engineering Research Institute
Sheffield Hallam University
Sheffield S1 1WB, UK

C. Semprebon
Smart Materials & Surfaces Laboratory, Faculty of Engineering & Environment
Northumbria University
Newcastle upon Tyne NE1 8ST, UK

K. E. Evans
Department of Engineering
University of Exeter
Exeter EX4 4QF, UK

## 1. Introduction

The shape and topography of surfaces have been a central focus in designing bespoke wetting properties into materials, often inspired by nature.[1–4] By creating a bed-of-nails effect mimicking the Lotus leaf, it is possible to create superhydrophobic surfaces, which ball-up droplets far beyond the ≈118° contact angle of Teflon possible with surface chemistry alone. By switching the surface chemistry to hydrophilic, such a surface can be converted to a hemi-wicking[5] or a superspreading surface.[6] Alternatively, by impregnating with a lubricating oil to replace the air in the lattice, it is possible to create a slippery liquid-infused porous surface (SLIPS) with virtually no resistance to droplet motion.[7,8] However, the prevailing paradigm in superhydrophobicity has been that the static arrangement of the lattice determines the solid surface fraction available to interact with a contacting liquid droplet and hence the wettability of the surface. There has been little attention to how the lattice structure may be reconfigured dynamically and the consequent effect on the wettability of the surface itself.

Simultaneously, in the field of metamaterials, there has been a realization of the profound importance that structure has in determining unusual material properties.[9–12] In particular, auxetic mechanical metamaterials have the counterintuitive property that when they are stretched they expand in an orthogonal direction.[13–16] Thus, unlike a conventional material, an auxetic lattice can expand by the creation of additional space (in both the direction of stretch and orthogonal to that direction) between its solid components, which do not themselves stretch or compress. Since the solid-to-air fraction at a surface controls extreme non-wetting and extreme wetting, auxetic materials would appear to be candidates for novel strain-controlled functional wetting materials.

Methods exist to fabricate auxetic metamaterials with structural features sufficiently small to explore the effect of their dynamic reconfiguration on the wettability of the metasurface itself. Rationally-designed metal, glass, and polymer-ordered auxetic microstructures with pore sizes down to ≈100 μm have been reported using soft lithography[17] and digital micromirror device projection printing,[18] for example. Laser micromachining, femtosecond-laser-induced two-photon polymerization, and

**ADVANCED
SCIENCE NEWS**

www.advancedsciencenews.com

**small
structures**

www.small-structures.com

dip-in direct-laser-writing optical lithography have been used to produce ordered auxetic metamaterials with pore sizes reduced to the range of 5–50 μm,[19–21] and pores sizes down to the nanoscale ($\approx$10 nm) have been reported in self-assembled auxetic periodic 2D protein lattices.[22] Disordered porous auxetics can be fabricated with pore sizes in the tens to hundreds of microns range including thermomechanical production of auxetic open-cell polymeric foams,[14] thermoforming powder processing of auxetic microporous polymers,[23] and papermaking of auxetic cellulosic fibrous mats.[24]

In this article, we hypothesize that, under tensile strain, an auxetic lattice necessarily reduces the solid fraction at the surface of a material and is capable of transforming that material into a superhydrophobic surface. To demonstrate our ideas, we formulate a mathematical model linking the structure of an auxetic surface to its wettability, which we then realize and validate experimentally.

## 2. Results and Discussion

### 2.1. Theoretical Fundamentals and Modeling

We start by considering a small liquid droplet on a perfectly flat and chemically smooth solid surface. Its equilibrium shape, determined by the balance of forces (or equivalently the minimum total interfacial energy) arising from the three interfacial tensions for the solid–gas, solid–liquid, and liquid–vapor interfaces, is that of a spherical cap which intersects the solid with the so-called Young's angle $\theta_Y$ (**Figure 1**a).[25] However, chemical and topographical heterogeneities on the solid introduce deviations from $\theta_Y$, and the droplet configuration is instead characterized by a static contact angle $\theta$ (Figure 1b). In general, the static contact angle is not unique, but is bounded by two limiting values, called the advancing and receding contact angles, $\theta_A$ and $\theta_R$, respectively. The advancing contact angle is defined as the largest angle that the droplet can attain before its contact line advances over the solid surface, e.g., upon an increase in its volume (Figure 1b). Similarly, the receding contact angle is the smallest angle that the droplet takes before the contact angle recedes from the solid. The fact that $\theta_A \neq \theta_R$ is indicative of pinning forces exerted by the solid on the droplet's contact line, and a measure of these forces is typically reported in terms of their difference, $\Delta\theta = \theta_A - \theta_R$, called the contact-angle hysteresis.[25]

Introducing a structure (or roughness) to a solid surface has a strong effect on its wettability because it alters the balance of the three interfacial forces.[26,27] For example, water tends not to penetrate small spaces between hydrophobic solid elements in the structure of a surface. A droplet can then be suspended on top of the structured surface and only partially in contact with it in a Cassie–Baxter state. Such a surface state is characterized by both the contact angle and the solid surface fraction, $f_S = A_S/A$, where $A_S$ is the solid surface area in contact with the droplet and $A$ is the planar projection of total surface area. In the case of a suspended droplet, the contact angle with the solid is referred to as the Cassie–Baxter contact angle, $\theta_{CB}$ (Figure 1c). In situations where the contact angle is $\approx$150° or higher, a regime achievable only for a Cassie–Baxter state, and a droplet can easily roll when the surface is tilted, the surface is referred to as superhydrophobic. Importantly, previous consideration of the change of wettability of surfaces with strain tends to assume elastic materials where the solid elements and the spaces between them both change size with strain, and experiments often use surfaces on which a droplet's contact line is pinned so that the droplet contact area and shape simply distorts to follow the strain pattern of the substrate.[28,29]

We now study the wettability of a structured solid surface (**Figure 2**), that exhibits both conventional and auxetic behaviour in response to an external force (Figure 2a,b). We start by considering a conventional hexagonal lattice with inextensible solid elements able to rotate about their connecting nodes in response to a mechanical force applied to the lattice (Figure 2c). When the lattice is stretched, the rotation of these solid elements at each lattice node causes the lattice to contract in the lateral direction[15] (Figure 2c). This is what we intuitively expect from experience with materials such as rubber strips. This behavior is naturally characterized in terms of the Poisson's ratio, $\nu$, defined as the negative ratio of the transverse strain ($\varepsilon_{lateral}$) to the longitudinal strain ($\varepsilon_{axial}$), in the direction of the loading force, i.e., $\nu = -\varepsilon_{lateral}/\varepsilon_{axial}$. Positive and negative strains correspond to extension and contraction, respectively. For a conventional hexagonal lattice, the transverse and longitudinal strains have opposite signs and the Poisson's ratio is, therefore, positive.

We now imagine a simple transformation of the hexagonal lattice into a bow-tie lattice by flipping the angles at two opposing nodes in each hexagonal unit (Figure 2c). When tensile strain is applied to the lattice, the rotation of the solid elements at each lattice node causes a counterintuitive expansion of the lattice in the lateral direction[15,30] (Figure 2c). Stretching a material or metamaterial causes an expansion of the surface area as long as $\nu < +1$ (see Supporting Information). Importantly for its
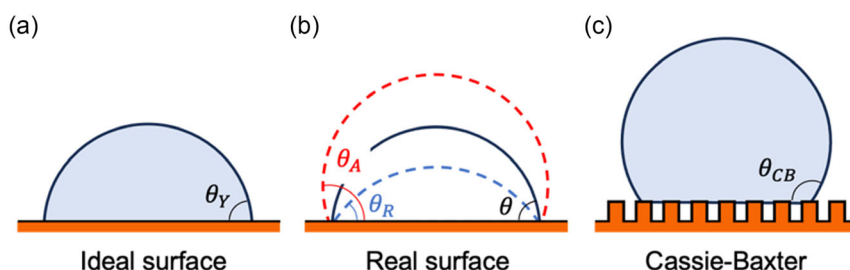


**Figure 1.** Wetting states of a droplet on a solid surface. a) Spherical-cap droplet intersecting an ideal solid surface with Young's angle. b) Droplet on a real surface, where the static angle is bounded by the advancing and receding contact angles. c) Cassie–Baxter state on a hydrophobic structured (or rough) surface.
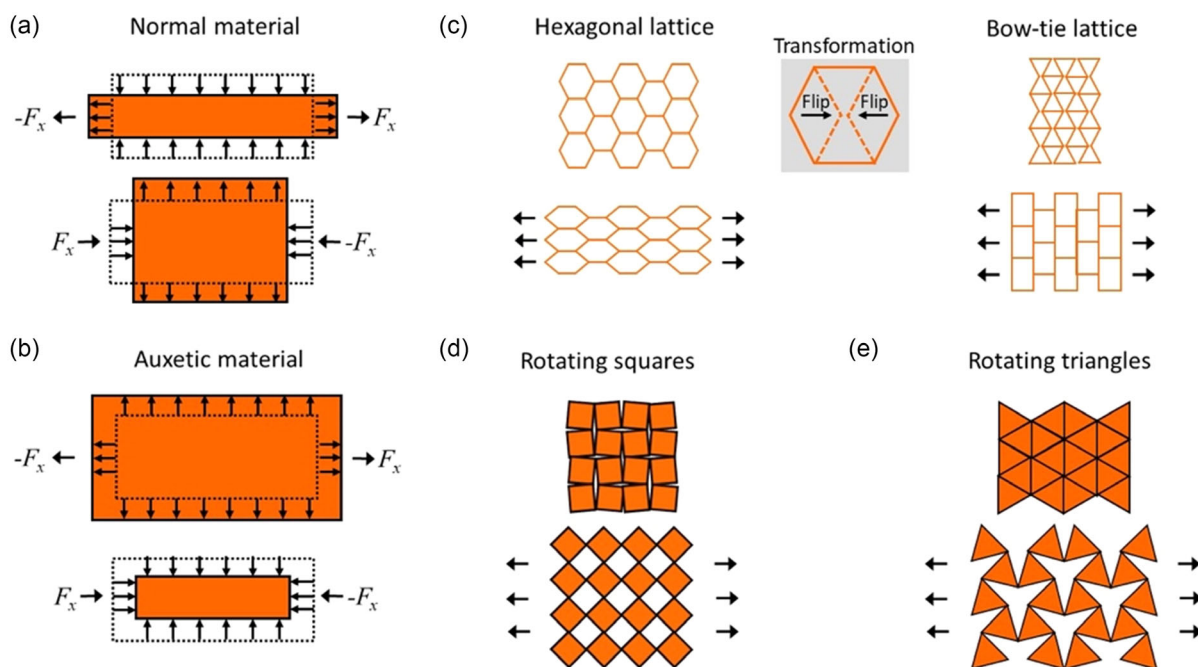
**Figure 2.** Auxetic metamaterial surfaces. Stretching and compression of a) a conventional material (positive Poisson's ratio) and b) an auxetic material (negative Poisson's ratio). c) Transformation of a conventional hexagonal lattice into an auxetic bow-tie lattice using rotation of rigid elements at nodal points.[15,17] Examples of rotating rigid shape-based auxetic materials. d) squares,[16,18] and e) triangles.[19] In each of the auxetic cases, tensile strain induces a systemic decrease in the solid surface fraction in the auxetic lattice.

wettability, the increase in surface area of the bow-tie metamaterial is through an expansion of the space, and not the solid, within the lattice. As a consequence, the solid surface fraction, $f_S$, also decreases as the metamaterial is stretched when $\nu < +1$ (this includes the stretch-induced transition from a bow-tie to a hexagonal geometry). Stretching the metamaterial further, i.e., for $\nu > +1$, causes a decrease in surface area, with the corresponding increase in solid surface fraction. From the perspective of nonwettable materials, an initially hydrophobic auxetic bow-tie lattice metamaterial supporting a droplet in a Cassie–Baxter suspended state will become systematically more hydrophobic and eventually superhydrophobic (including the minimum in solid surface fraction following the transition to a positive Poisson's ratio for a hexagonal lattice), before returning to a hydrophobic state upon further stretching. Similarly, it is possible to imagine new and unique superhydrophilic wettable, hemiwicking, and liquid-infused auxetic materials.

Our concept for the wetting properties of auxetic metamaterials applies to a wide range of lattice structures and is not limited uniquely to bow-tie lattices. Another class of auxetic metamaterials uses tessellations of two-dimensional shapes connected at their corners so that each shape can rotate cooperatively about their corners. Thus, for example, a set of corner-connected rigid squares,[16,31] as shown in Figure 2d, rotates under strain into a diamond-shaped lattice with a Cassie solid surface fraction, $f_S$, systematically decreasing from unity to 0.5. Other similar designs using, e.g., triangles[32] (Figure 2e), also behave in an auxetic manner under strain. We therefore observe that there are many classes of auxetic metamaterials whose surface wettability will change in a uniquely defined manner with strain.

We next model the solid surface fraction of a bow-tie auxetic surface with rotatable inextensible solid elements under tensile strain in the vertical ($x_2$) direction (**Figure 3**a, Supporting Information Figure S6). The Poisson's ratio for this geometry has been derived previously to be $\nu_{21} = \sin\alpha(h_u/l_u + \sin\alpha)/\cos^2\alpha$ (geometrical parameters defined in the Supporting Information), where the subscript refers to the loading ($x_2$) and transverse ($x_1$) directions. For simplicity, in the following, $\nu \equiv \nu_{21}$. As the strain, $\varepsilon = \Delta L_{\text{axial}}/L_{\text{axial}}$, where $\Delta L_{\text{axial}}$ is the change in the axial length $L_{\text{axial}}$ (and, in this case, $L_{\text{axial}}$ corresponds to the unit cell length $X_2$ in the Supporting Information) increases, the opposing arms of each bow-tie straighten (i.e., the negative value of $\alpha \rightarrow 0°$) and eventually an entirely rectangular lattice ($\alpha = 0°$) is achieved. Beyond this point, the angles at the two opposing nodes of each bow-tie shape invert to create a conventional hexagonal lattice ($\alpha > 0°$). The solid surface fraction, $f_s$, systematically decreases with strain until a minimum, which is always within the conventional lattice region, when $\nu = +1$, is reached (Figure 3a; see Supporting Information for a proof). The corresponding Cassie–Baxter contact angle, $\theta_{\text{CB}}$, of a droplet suspended on this geometry, is shown in Figure 3b (see Supporting Information for model parameters). Here, $\theta_{\text{CB}}$ is defined through the weighted average $\cos\theta_{\text{CB}} = f_s\cos\theta_S + (1-f_s)\cos\theta_A$, where $\theta_S$ is the contact angle of a droplet on a hydrophobic solid, e.g. $\theta_S = 120°$ and $\theta_A = 180°$ (i.e., $\cos\theta_A = -1$) represents the contact angle of a droplet on air. As strain is applied, the auxetic surface transforms from hydrophobic ($\theta_{\text{CB}} < 150°$) to superhydrophobic ($\theta_{\text{CB}} > 150°$) before becoming a conventional (nonauxetic), but still superhydrophobic surface. Eventually, a maximum in superhydrophobicity is

ADVANCED
SCIENCE NEWS
www.advancedsciencenews.com

small
structures
www.small-structures.com
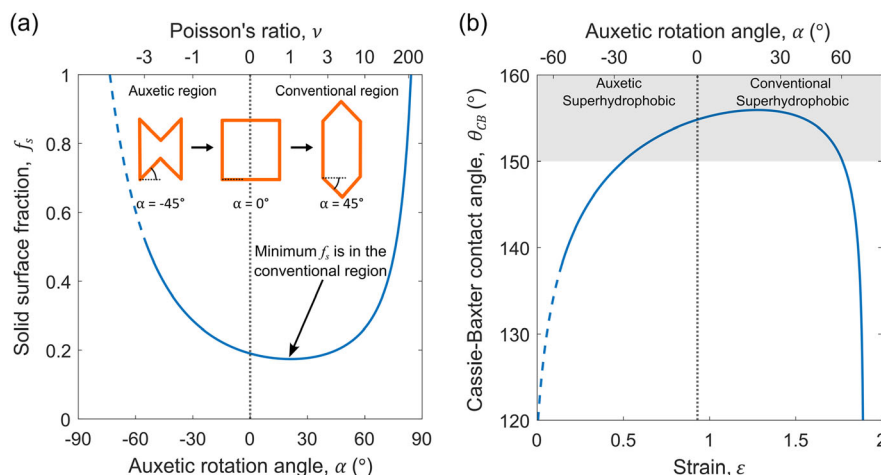
**Figure 3.** Model strain dependence of a hydrophobic auxetic surface. a) Predicted changes of solid surface fraction, $f_s$, with auxetic rotation angle, $\alpha$. The initially auxetic bow-tie lattice is transformed into a conventional hexagonal lattice for positive auxetic rotation angle, as indicated by the Poisson's ratio, $\nu$ (top axis). The minimum solid surface fraction occurs in the conventional lattice region when $\nu = +1$. b) Predicted Cassie–Baxter contact angle, $\theta_{CB}$, for suspended state droplets with applied tensile strain, $\varepsilon$. Strain-induced superhydrophobicity occurs for both the auxetic and conventional regions, but there is a unique value of contact angle for each value of strain in the auxetic case. The zero of strain has been defined to correspond to a closed auxetic lattice with the maximum solid surface fraction, $f_s$. Model parameters are detailed in the Supporting Information.

achieved before the lattice closes up and the material reverts to being a hydrophobic, but conventional surface. This reveals a unique property of the auxetic superhydrophobicity arising from the monotonic decrease in solid surface fraction with increasing strain. There is only ever a single value of strain for any one value of the Cassie–Baxter contact angle in the auxetic region. In contrast, the existence of a minimum solid surface fraction in the conventional region means a single value of Cassie–Baxter contact angle can correspond to either a strain above or a strain below that which characterizes the maximum.

## 2.2. Experiments

To experimentally confirm the relation between lattice configurations at different states of strain and the wettability of the surface, we constructed a set of physical models (Supporting Information). This enables direct comparison of the wetting response of the physical models with the predicted response of a honeycomb with rotatable inextensible solid elements under tensile strain, as opposed to straining a single physical model which would also be subject to flexing and stretching of the solid elements not accounted for in the predictive model used here. Our models used a polymer (SU-8) photolithographically patterned into bow-tie lattice microstructures with solid surface fractions chosen to represent the full set of configurations across a strain curve (**Figure 4**a). Each lattice was treated with a low-pinning hydrophobic coating, which gives advancing and receding contact angles $\theta_A = 105.2°$ and $\theta_R = 102.5°$ on a flat control surface, although different degrees of pinning could be achieved using the same coating (see Supporting Information). By choosing the height of the walls ($\approx 60\,\mu m$) to be larger than the typical void between the walls, penetration of water into the structure is inhibited, favoring a Cassie-suspended droplet state. Figure 4b shows representative profile images of droplets in contact with

the surfaces of these structures. The characterization of the wetting of these structures shows a systematic increase in the static contact angles, $\theta$, and, hence, hydrophobicity, as the lattices transition from bow-tie to rectangular, representing auxetic states (Figure 4c). Because the bow-tie lattice design is asymmetric, we report contact angles from two orthogonal viewing directions (Figure 4c, inset), as well as their average. For large, positive $\alpha$ (e.g., $\alpha = 75°$ in Figure 4a), the contact angle measured along orientation II is always smaller, suggesting that the droplet is able to spread more easily along the direction of the solid elements. Notably, this property is reversed as the geometry crosses over to the auxetic region. A maximum corresponding to an extreme nonwetting contact angle of $\approx 150°$ with a droplet in a suspended state is observed in the conventional (hexagonal) lattice region before falling rapidly as the lattice closes up and the solid surface fraction increases. The two continuous curves show the predicted hydrophobicity for these lattice designs using the Cassie–Baxter model with the advancing and receding contact angles of 105.2° (upper curve) and 102.5°, respectively. These correspond to the lower and upper bounds expected from the theory and show a remarkable agreement with experimental results.

Next, we developed a process to create micropatterned polydimethylsiloxane (PDMS) membranes with auxetic surface-wetting properties (Supporting Information). A layer of a photoresist (SPR220-7) was spin-coated to create a film on a silicon wafer and then patterned to a depth of $\approx 20\,\mu m$ using exposure to ultraviolet light. PDMS was then spin-coated across the pattern and cured. Subsequently, the excess above the pattern was etched away to expose the lattice ribs. A final soak in acetone dissolved the photoresist releasing the auxetic PDMS membranes. These membranes were mounted in a microstretching apparatus and observed from above to confirm auxetic behavior (**Figure 5**a and Supporting Information: Video 1). Droplets in contact with these membranes tended to penetrate into the void spaces
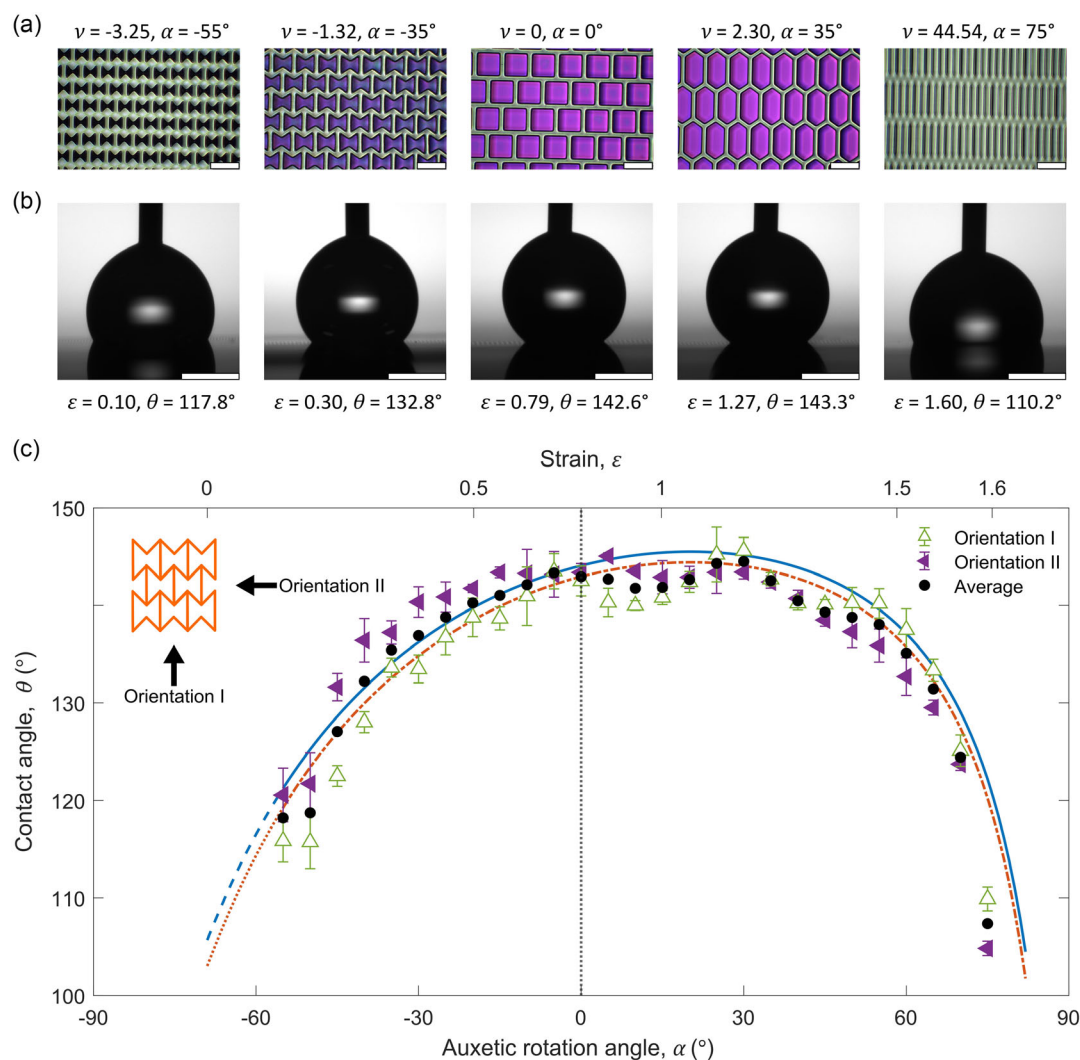
**Figure 4.** Model of a hydrophobic auxetic surface. a) Top images of low-pinning hydrophobic surfaces representing different strained states of a bow-tie lattice (scale bar 100 µm). b) Side profile images of water droplets in contact with the surfaces (scale bar 500 µm). c) Data for contact angle viewed from two orthogonal directions (Inset: Orientation I and II). Continuous curves show model predictions using the lattice design parameters and the measured advancing and receding contact angles on a flat control surface (upper and lower curves, respectively). The dashed and dotted portions of the curves indicate values of the angle for which lattice solid elements overlap.

between membrane ribs even when hydrophobized with fluorosilane (Figure 5b). This could be prevented using a super-hydrophobic nanoparticle coating (Figure 5c), but doing so created a completely nonadhesive surface onto which a droplet could not be detached onto the membrane from the syringe (Supporting Information: Video 2). When droplets were deposited onto such a superhydrophobic membrane, the contact angle was insensitive to the level of strain applied (Supporting Information Figure S5). Since the rigidity of a thin sheet scales with the cube of its thickness, these membranes have little rigidity normal to their surface, and elastocapillary effects[33,34] are observed with the droplet bending the membranes out of plane (Figure 5b). Such an effect could offer the opportunity to use the synclastic (double) curvature[14,30,35] of an auxetic membrane to wrap a droplet surface[33] without causing wrinkling or creasing.

## 3. Conclusion

We now return to the contrasting ideas that metamaterials are materials with properties that are uncommon, but that superhydrophobic surfaces are themselves inspired by nature. Natural biological systems grow and their surfaces have to adapt both to the change in curvature of their surfaces and to the environment in which they live, which is often water or a partially wet or water-clogged material. A common adaptation of insects to breathing underwater is the use of breathing holes with a surface-attached layer of air (a "plastron")[36] whose air–water interface acts as an oxygen–carbon dioxide exchange membrane. The plastron is a naturally occurring feature when a superhydrophobic material is immersed in water. In the case of insects such as *Orchesella cincta*,[37] a type of springtail (Collembola) that lives in water-logged ground, the plastron is achieved with
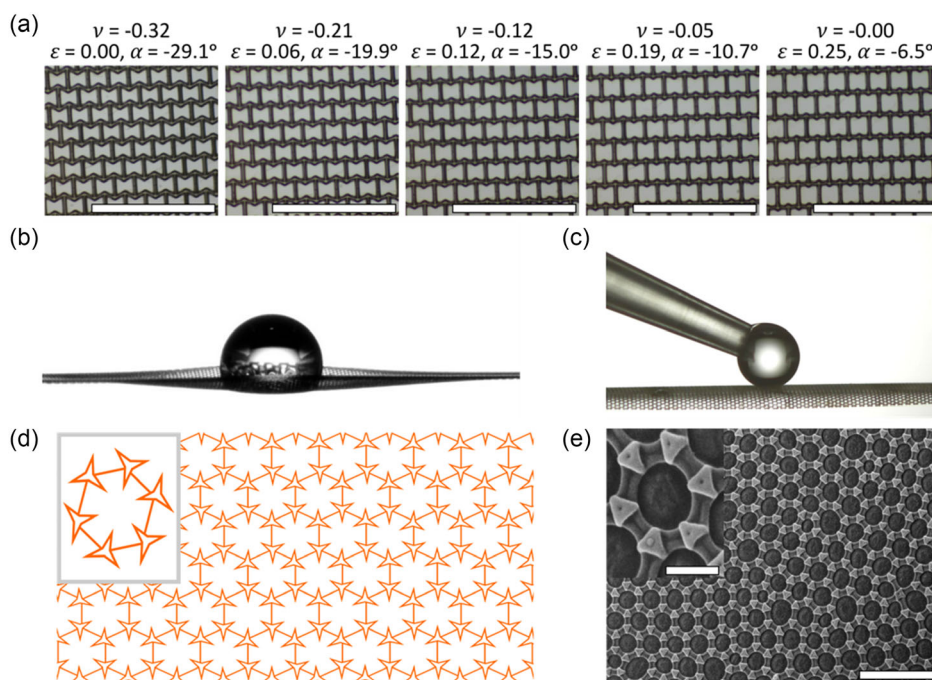
**Figure 5.** Auxetic membranes. a) Top images of an auxetic fluorosilanized PDMS membrane in different states of strain with corresponding auxetic rotation angle and Poisson's ratio values (scale bar 500 µm). Side profile images of water droplets in contact with the surface of b) an auxetic fluorosilanized PDMS membrane, and c) an auxetic PDMS membrane possessing a superhydrophobic nanoparticle coating. The membrane in b) is distorted out of plane by elastocapillary forces due to the strength of the surface tension forces from the droplet. d) An auxetic lattice pattern which resembles the structure observed on e) the cuticle water-repelling surface of the soil-dwelling springtail *Orchesella cincta*[37] (SEM images provided by A. E. Filippov; scale bars in the main image and the detail are 1 µm and 200 nm, respectively).

hydrophobic surface features which prevent the breathing holes from being flooded. It is therefore interesting to contrast images of the cuticle surface of the springtail with a classic connected star-type auxetic design[38] (Figure 5d,e). We note that, although different from the hexagonal lattice studied in this article, such a design possesses similar properties in achieving a variation of the solid surface fraction upon a reconfiguration induced by strain. It is possible that the springtail exoskeleton has adapted such that as the underlying surface stretches the star-shaped surface feature spacing expands in an auxetic manner or alternatively an auxetic expansion is achieved by the straightening of the edges on each star-shaped surface feature. Although studies of this geometry are beyond this work, we believe these observations should motivate a wider search for naturally occurring auxetic wetting properties in biological systems.

The transformation of a metamaterial into a superhydrophobic surface and the use of metamaterial concepts for the design and control of wetting are a hitherto unrecognized opportunity for new types of material surfaces with unique properties. Here, we have used auxetic principles to create strain-controlled hydrophobicity and superhydrophobicity exemplified by lattice models and membranes. These principles can be extended to other types of auxetic lattices. They will also apply to the wetting of the surfaces of structure-independent auxetic materials with unknown geometries, but known elastic properties, such as shape memory foams, provided they have small pores, such that interfacial tension forces dominate. Such materials can also provide increased robustness against continued actuation, thus opening a route

toward practical applications. We have also suggested that the uncommon properties of metamaterial wettability might have natural examples. The design principles presented here provide a foundation for new types of surfaces relevant to superwater repellent applications,[39] liquid encapsulation,[33,40] and microreactors,[41,42] and may also have an application to strain controllable liquid–liquid separations[43] or droplet catch-and-release.[44]

## Supporting Information

Supporting Information is available from the Wiley Online Library or from the author.

## Acknowledgements

## Conflict of Interest

The authors declare no conflict of interest.

## Data Availability Statement

The data that support the findings of this study are available from the corresponding author upon reasonable request.

## Keywords

[1] C. Neinhuis, W. Barthlott, *Ann. Bot.* **1997**, *79*, 667.

[2] W. Barthlott, C. Neinhuis, *Planta* **1997**, *202*, 1.

[3] T. Sun, L. Feng, X. Gao, L. Jiang, *Acc. Chem. Res.* **2005**, *38*, 644.

[4] B. Bhushan, Y. C. Jung, *Prog. Mater. Sci.* **2011**, *56*, 1.

[5] J. Bico, C. Tordeux, D. Quéré, *Europhys. Lett.* **2001**, *55*, 214.

[6] G. McHale, N. J. Shirtcliffe, S. Aqil, C. C. Perry, M. I. Newton, *Phys. Rev. Lett.* **2004**, *93*, 036102.

[7] T.-S. Wong, S. H. Kang, K. Y. Tang, E. J. Smythe, B. D. Hatton, A. Grinthal, J. Aizenberg, *Nature* **2011**, *477*, 443.

[8] A. Lafuma, D. Quéré, *Europhys. Lett.* **2011**, *96*, 56001.

[9] J. B. Pendry, *Phys. Rev. Lett.* **2000**, *85*, 3966.

[10] Z. G. Nicolaou, A. E. Motter, *Nat. Mater.* **2012**, *11*, 608.

[11] M. Kadic, T. Bückmann, R. Schittny, M. Wegener, *Rep. Prog. Phys.* **2013**, *76*, 126501.

[12] T. A. M. Hewage, K. L. Alderson, A. Alderson, F. Scarpa, *Adv. Mater.* **2016**, *28*, 10323.

[13] K. E. Evans, M. A. Nkansah, I. J. Hutchinson, S. C. Rogers, *Nature* **1991**, *353*, 124.

[14] R. S. Lakes, *Science* **1987**, *235*, 1038.

[15] K. E. Evans, A. Alderson, *Adv. Mater.* **2000**, *12*, 617.

[16] R. S. Lakes, *Annu. Rev. Mater. Res.* **2017**, *47*, 63.

[17] B. Xu, F. Arias, S. T. Brittain, X.-M. Zhao, B. Grzybowski, S. Torquato, G. M. Whitesides, *Adv. Mater.* **1999**, *11*, 1186.

[18] D. Y. Fozdar, P. Soman, J. W. Lee, L.-H. Han, S. Chen, *Adv. Funct. Mater.* **2011**, *21*, 2712.

[19] U. D. Larsen, O. Sigmund, S. Bouwstra, *J. Microelectromech. Syst.* **1997**, *6*, 99.

[20] W. Zhang, P. Soman, K. Meggs, X. Qu, S. Chen, *Adv. Funct. Mater.* **2013**, *23*, 3226.

[21] T. Bückmann, N. Stenger, M. Kadic, J. Kaschke, A. Frölich, T. Kennerknecht, C. Eberl, M. Thiel, M. Wegener, *Adv. Mater.* **2012**, *24*, 2710.

[22] Y. Suzuki, G. Cardone, D. Restrepo, P. D. Zavattieri, T. S. Baker, F. A. Tezcan, *Nature* **2016**, *533*, 369.

[23] K. L. Alderson, K. E. Evans, *Polymer* **1992**, *33*, 4435.

[24] P. Verma, M. L. Shofner, A. C. Griffin, *Phys. Status Solidi B* **2014**, *251*, 289.

[25] P. G. de Gennes, *Rev. Mod. Phys.* **1985**, *57*, 827.

[26] A. B. D. Cassie, S. Baxter, *Trans. Faraday Soc.* **1944**, *40*, 546.

[27] D. Quéré, *Annu. Rev. Mater. Res.* **2008**, *38*, 71.

[28] D. Wang, Y. Liu, S. Sridhar, Y. Li, G. McHale, H. Lu, Z. Yu, S. Wang, B. B. Xu, *Adv. Mater. Interf.* **2021**, *8*, 2001199.

[29] M. Coux, C. Clanet, D. Quéré, *Appl. Phys. Lett.* **2017**, *110*, 251605.

[30] A. Alderson, K. L. Alderson, *Proc. Inst. Mech. Eng. Part G: J. Aerosp. Eng.* **2007**, *221*, 565.

[31] J. N. Grima, K. E. Evans, *J. Mater. Sci. Lett.* **2000**, *19*, 1563.

[32] J. N. Grima, R. Jackson, A. Alderson, K. E. Evans, *Adv. Mater.* **2000**, *12*, 1912.

[33] C. Py, P. Reverdy, L. Doppler, J. Bico, B. Roman, C. N. Baroud, *Phys. Rev. Lett.* **2007**, *98*, 156103.

[34] J. Bico, É. Reyssat, B. Roman, *Annu. Rev. Fluid Mech.* **2018**, *50*, 629.

[35] K. E. Evans, *Compos. Struct.* **1991**, *17*, 95.

[36] D. J. Crisp, W. H. Thorpe, *Discuss. Faraday Soc.* **1948**, *3*, 210.

[37] A. E. Filippov, A. Kovalev, S. N. Gorb, *J. R. Soc. Interface* **2018**, *15*, 20180217.

[38] J. N. Grima, R. Gatt, A. Alderson, K. E. Evans, *Mol. Simul.* **2005**, *31*, 925.

[39] Y. Liu, L. Moevius, X. Xu, T. Qian, J. M. Yeomans, Z. Wang, *Nat. Phys.* **2014**, *10*, 515.

[40] G. McHale, M. I. Newton, N. J. Shirtcliffe, N. R. Geraldi, *Beilstein J. Nanotechnol.* **2011**, *2*, 145.

[41] G. McHale, M. I. Newton, *Soft Matter* **2015**, *11*, 2530.

[42] N. K. Nguyen, C. H. Ooi, P. Singha, J. Jin, K. R. Sreejith, H. P. Phan, N. T. Nguyen, *Processes* **2020**, *8*, 793.

[43] Z. Xue, Y. Cao, N. Liu, L. Feng, L. Jiang, *J. Mater. Chem. A* **2014**, *2*, 2445.

[44] A. Laroche, A. Naga, C. Hinduja, A. A. Sharifi, A. Saal, H. Kim, N. Gao, S. Wooh, H.-J. Butt, R. Berger, D. Vollmer, *Droplet* **2023**, *2*, e42.